



Research Article

Chemical and boron isotope composition of multiple generations of tourmaline from the Nassarawa lithium-rich pegmatites, Nigeria: Implications for the mechanism of lithium enrichment

Junteng Lv ^a, Xin Chen ^{a,*}, Junsheng Jiang ^{b,*}, Hans-Peter Schertl ^c, Liang Cao ^b, Xiaojia Jiang ^a

^a State Key Laboratory of Geological Processes and Mineral Resources and School of Earth Resources, China University of Geosciences, Wuhan 430074, China

^b Wuhan Center, China Geological Survey (Central South China Innovation Center for Geosciences), Wuhan 430205, China

^c Ruhr-University Bochum, Faculty of Geosciences, Institute of Geology, Mineralogy and Geophysics, 44780 Bochum, Germany

ARTICLE INFO

Keywords:

Pulsed melts
Magma evolution
Boron isotopes
Magmatic reservoir
Pegmatites

ABSTRACT

Pegmatites are the primary global source of rare metal lithium (Li). While previous studies highlight the importance of high granitic magma differentiation in the formation of lithium-rich pegmatites, the processes and timescales of magmatic fractionation remain unclear. Specifically, it is uncertain whether lithium-rich melts originate from multiple magmatic pulses or a single continuous fractional crystallization event. This study presents elemental mapping, in-situ trace element analysis, and boron isotope data for four generations of tourmaline sourced from the lithium mineralization of the Nassarawa-Keffi pegmatitic belt in Nigeria. Tourmaline grains intergrowth with plagioclase, quartz, and K-feldspar, display compositional zoning and resorption-precipitation textures, indicating incremental growth predominantly influenced by the injection of multistage magma batches. The notable periodic increases in Li and Mn contents, accompanied by decreases in Fe, as well as the distinct variation trends in the Li/Sc, Li/K, and Li/Ge ratios across the four tourmaline generations, suggest the involvement of at least four distinct melt pulses. The narrow $\delta^{11}\text{B}$ values observed across all tourmaline generations indicate a single magmatic source. The observed decrease in $\delta^{11}\text{B}$ values in the later tourmaline generations is likely due to fluid exsolution and mineral crystallization processes. Subsequent magma pulses exhibit higher lithium concentrations than earlier, suggesting that multistage melt pulses and high fractional crystallization within a deep magmatic reservoir are essential for lithium enrichment in the Nassarawa lithium-rich pegmatites. Based on these findings, we propose an alternative model in which multiple melt-release events from a single cooling magmatic reservoir contribute to the formation of lithium-rich pegmatites.

1. Introduction

Granitic pegmatites are crucial sources of rare metals, including Li, Be, Nb, Ta, and Sn (Černý, 1991; Černý and Ercit, 2005; Fan et al., 2022; Kesler et al., 2012). These pegmatites, associated with varying mineralization types, are often interpreted either as residual melts extracted from a large granitic magma reservoir (Černý and Ercit, 2005; Xiong et al., 2024) or as products of the partial melting of metal-rich continental crustal rocks (Koopmans et al., 2023; Müller et al., 2017). Both models underscore the significance of fractional crystallization in the formation of lithium-rich pegmatites (Cameron et al., 1949; Černý, 1991; Knoll et al., 2023; Wu et al., 2020). Unzoned Li-rich pegmatite, which typically contains mineralization types such as Li, Nb, and Ta, is

often referred to as fully mineralized Li-rich pegmatite. However, it remains unclear whether these mineralization types formed simultaneously or in a specific sequence. A key issue revolves around the timescale and mechanisms of lithium-rich melt formation, particularly whether these melts develop through intermittent enrichment from multiple pulses or from a continuous fractional crystallization process.

The traditional view of granitic melt release from deep magmatic reservoirs for the formation of granite and pegmatite suggests a continuous process (Cameron et al., 1949; Daly, 1911; Jahns and Burnham, 1969). This magma evolution, driven by crystal fractionation and influenced by changes in melt composition, temperature, and pressure, can generate extensive mineralized zones that transition from core to rim within granite and pegmatite bodies (Bradley and McCauley,

* Corresponding authors.

E-mail addresses: chenxin68@cug.edu.cn (X. Chen), jsjiang0818@163.com (J. Jiang).

2013). Typically, the highly fractionated melts, which are enriched in incompatible elements like Li and Be, are found in the cores of pegmatite bodies, while less fractionated materials are located in the rims or within the larger, deeper magmatic reservoirs (Cameron et al., 1949). However, the presence of unzoned, fully mineralized pegmatite bodies—such as those observed in North and South Carolina, Jiajika, and Qiongjiagang—presents a challenge to this model, particularly due to the lack of distinct textural features (Liu et al., 2024; Swanson, 2012; Yang et al., 2020). In contrast, geophysical, geochemical, petrological, volcanological, and geological evidence for melt injection processes is well-documented in various magmatic systems (Cashman et al., 2017; Coleman et al., 2016). This evidence is especially evident in the development of multistage granite systems, episodic growth of lava domes, and cross-cutting pegmatite veins observed in numerous deposits (Annen, 2009; Chen et al., 2022; Coleman et al., 2016; Menand, 2011; Swanson, 2012; Vigneresse, 2008). While pulsed magma processes are widely accepted in the context of igneous rocks (Coleman et al., 2016; Vigneresse, 2015), the applicability of these processes to the formation of granitic pegmatites requires further investigation. Understanding the magmatic processes that lead to pegmatite formation poses inherent challenges due to the restricted spatial volume and the coarse-grained nature of pegmatite minerals. This complexity makes it difficult to determine bulk elemental and isotopic compositions, which may not fully represent the characteristics of the magma. The key challenge lies in identifying the multi-stage growth domains of minerals that formed during the evolution of magmatic systems. This understanding is essential for elucidating the geochemical changes that occur during the development of lithium-rich granitic melts as they ascend from deep-seated magmatic reservoirs to shallower crustal levels.

In an endeavor to unravel the evolution of magmatic melt releases for the formation of lithium-rich pegmatites as either a pulsed phenomenon or a continuous event, this study recently discovered multistage tourmaline specimens exhibiting zones of varying lithium contents in the Nassarawa rare metal pegmatite belt, Nigeria (Akintola et al., 2012; Cao et al., 2024; Okunola and Somorin, 2006). The research employs elemental mapping, trace element geochemistry, and boron isotope studies of tourmaline as proxies to illustrate the composition, source, and evolution of multistage melts originating from a cooling magma chamber over time and to provide insights into the mechanism of lithium enrichment.

2. Geological background and samples

Nigeria is located in the central-western part of Africa (Fig. 1a) and is composed of four main geological formations: crystalline basement, Neoproterozoic granitoids, Mesozoic granitoids, and Mesozoic to recent sedimentary cover units (Fig. 1b; Vincent et al., 2022). The crystalline basement, also referred to as the Nigerian Shield, is partitioned into eastern and western terranes (Ajibade et al., 1987; Ananaba and Ajakaiye, 1987; Ferré et al., 1996; Fitches et al., 1985). Nigerian Shield comprises a gneissic migmatite complex exhibiting amphibolite-facies metamorphism and a Paleoproterozoic schist belt trending in the north-south direction, which is intruded by Neoproterozoic and Mesozoic granitoids (Fig. 1b; Ajibade et al., 1987; Arthaud et al., 2008; Bruguier et al., 1994; Fitches et al., 1985). The Neoproterozoic granitoids display syn-collisional and post-collisional characteristics; their formation age is between 750 and 580 Ma coinciding with the assembly of the western portion of Gondwana during the Late Neoproterozoic to Early Cambrian transition (Adetunji and Ocan, 2010; Goodenough et al., 2014). Pegmatites with significant Li-Nb-Ta-Be-Sn mineralization are present in the NNE-SSW trending belt within the eastern basement (Fig. 1b; Akintola et al., 2012; Okunola and Somorin, 2006; Vincent et al., 2022). U-Pb dating of cassiterite from these Nb-Ta-, Be-, and Li-rich pegmatites reveals that these rare metal-rich pegmatites primarily formed between approximately 572 and 548 Ma, corresponding to the Gondwana-forming orogeny (Cao et al., 2024).

The Nassarawa-Keffi area is situated in the middle of the Nigerian Li-Nb-Ta-Be-Sn mineralized pegmatite belt (Fig. 1c). The major geological unit is composed of gneissic migmatites, granitic gneiss, and schists intruded by Neoproterozoic granites and pegmatites (Fig. 1b). The surface is widely covered by Quaternary sediments and pegmatites are in mine adits (Fig. 2a). The unzoned pegmatites occur as near vertical dykes, predominantly striking NNE-SSW. They have intruded pre-existing lithologies of granitic gneiss and schists irregular to sharp boundaries (Fig. 2a). The Li-rich unzoned pegmatites (sample numbers BY2) crop out in the southern Nassarawa area without obvious mineralization zones around the Ombi-Imu granite (Fig. 1b). Pegmatites in this area are rich in Li, Nb and Ta and intruded granitic gneiss and schists. Columbite and cassiterite are present in weathered clay layers altered pegmatites (Fig. 2a and d). The samples from this study were collected from a small mine adit about 10 km south of Nassarawa, currently being mined by local residents (Figs. 2a). This Li-rich unzoned pegmatite is distinguished by the presence of primary minerals:

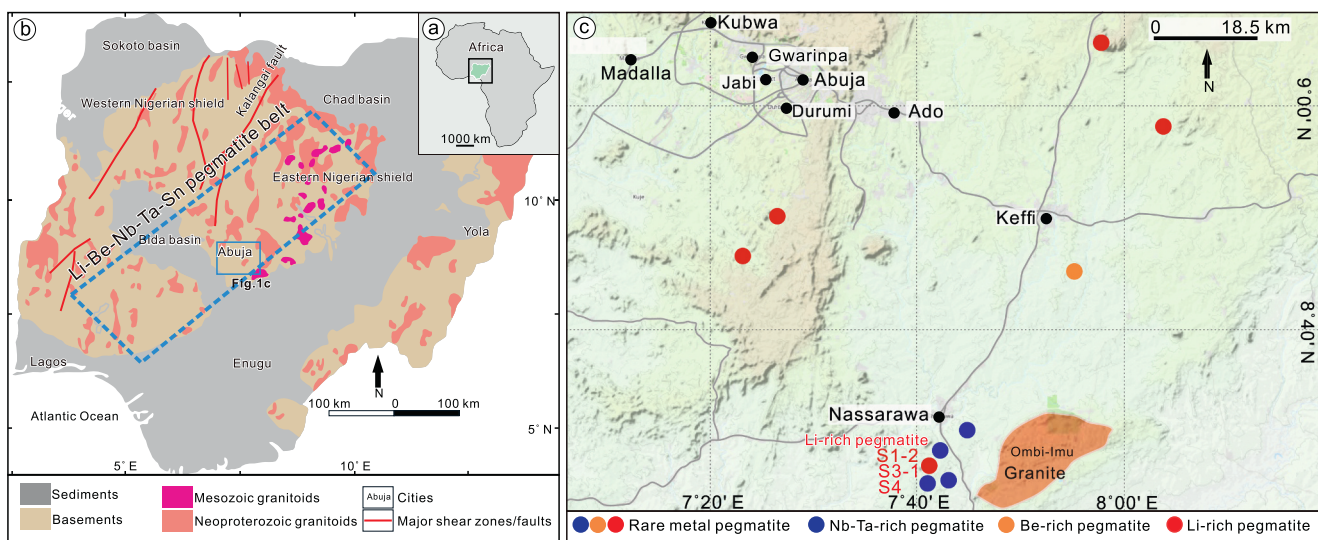


Fig. 1. (a) The location of Nigeria in Africa; (b) Simplified geological map of the Nigeria, modified from (Dada, 1998; Goodenough et al., 2014); (c) The location of lithium-rich pegmatite samples in the Nassarawa area.

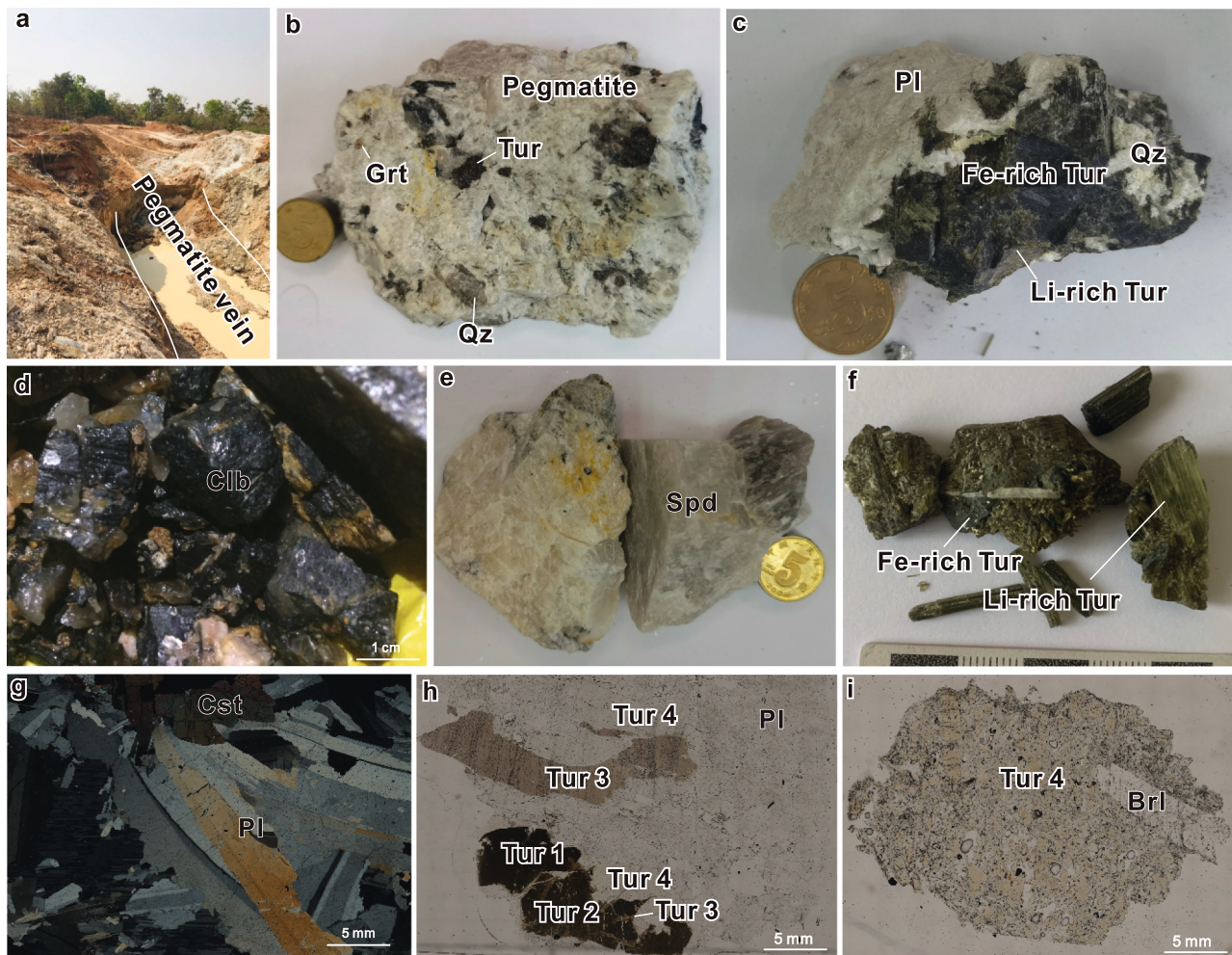


Fig. 2. Photographs of Li-rich pegmatite in the Nassarawa area. (a) The pegmatite vein hosted in the mica schist and quartzite; (b-f) The Li-rich pegmatite with Fe-rich and Li-rich tourmaline, quartz, garnet, plagioclase, spodumene and columbite; (d) Cassiterite intergrow with plagioclase in the Li-rich pegmatite; (e) Four generations of tourmaline with different color in the Li-rich pegmatite; (i) Tur 4 intergrowth with beryl. Grt-garnet; Tur-tourmaline; Pl-plagioclase; Oz-quartz; Crb-columbite; Spd-spodumene; Cst-cassiterite; Brl-beryl.

tourmaline, garnet, muscovite, quartz, plagioclase, K-feldspar, spodumene, coarse-grained columbite, and cassiterite (Fig. 2). Some coarse-grained columbite crystals can reach 5 cm in size (Fig. 2d), and cassiterite with plagioclase can reach 5 cm (Fig. 2g). Spodumene crystals associated with plagioclase and quartz show grain sizes up to 10 cm and display typical {110} cleavage under the polarizing microscope (Fig. 2e).

3. Analytical method

The element mapping of the tourmaline generations was performed using a Tescan Integrated Mineral Analyzer (TIMA) mineralogy system at Guangzhou Tuoyan Analytical Technology Co., Ltd. This analysis aimed to verify complex mineral relationships. An acceleration voltage of 25 kV, a probe current of 8.24 nA, and a pixel size of 3.5 μm were employed on the same MIRA3 FE-SEM for the BSE images. The spacing between points for energy-dispersive spectrometry (EDS) analyses was 10.5 μm .

The major and trace element concentrations of the four tourmaline generations were analyzed utilizing a NWR 193 HE laser ablation system coupled to an Agilent 7900 single quadrupole ICP mass spectrometer at the LA-ICP-MS laboratory located in the Collaborative Innovation Center for Exploration of Strategic Mineral Resources, China University of Geosciences (Wuhan). Helium served as the carrier gas for sample

ablation. Each spot analysis included approximately 30 s of background acquisition followed by 40 s of data acquisition. A spot size of 32 μm was employed, along with a repetition rate of 8 Hz and an energy density of approximately 3.5 J cm^{-2} . Every 8–10 sample analyses several analyses on external reference material were carried out. NIST SRM 610 was utilized as the quality control (QC) reference material to correct instrumental time-dependent sensitivity drift, while multiple external standards (NIST 610, NIST 612, BCR-2G, BHVO-2G, and BIR-1G) were selectively employed for external calibration (Liu et al., 2008). Off-line selection and integration of background and analyzed signals, time-drift correction, and quantitative calibration for trace element analysis were performed using an Excel-based software, ICPMSDataCal 10.9 (Liu et al., 2008). The major and trace element data for the tourmaline generations determined using LA-ICP-MS, are listed in Table S1.

A RESolution S155-LR 193 nm laser ablation system, paired with a Neptune plus multi-collector inductively coupled plasma mass spectrometer (LA-MC-ICP-MS), was used for in situ analysis of B isotopes in tourmaline at the Laboratory of Isotope Geochemistry, Wuhan Center of China Geological Survey. A laser beam spot diameter of 43 μm was chosen with an energy density of 3.5 J/cm² and a frequency of 5 Hz. Quality fractionation correction on the data was performed using the Sample-Standard Bracketing (SSB) method, which involved analyzing a standard sample before and after each test sample. The average mass discrimination of the standard sample was then applied to correct the

test results of the samples. This laboratory employs the standard material IMR-RB1, developed by the Institute of Mineral Resources, Chinese Academy of Geological Sciences, for external standard correction of data quality fractionation. Samples 112,566-Schorl and 98,144-Elbaite were used as monitoring samples to control the quality of the data, with each monitored once for every 5 sample points. The boron isotope compositions of $\delta^{11}\text{B}$ reference values for IMR-RB1, 112,566-Schorl, and 98,144-Elbaite were $-12.2 \pm 1.1\text{‰}$, $-12.5 \pm 0.1\text{‰}$, and $-10.5 \pm 0.2\text{‰}$, respectively (Hou et al., 2010; Ishikawa et al., 2001; Ishikawa and Tera, 1997). Monitoring samples 112,566-Schorl and 98,144-Elbaite yielded results of $-12.4\text{‰} \pm 0.6\text{‰}$ ($n = 40, 2\sigma$) and $-10.5\text{‰} \pm 0.6\text{‰}$ ($n = 24, 2\sigma$), respectively, consistent with the reference values within the error range. The boron isotope compositions of the four generations of tourmaline are listed in Table S2.

4. Results

4.1. Petrography and major elemental compositions

Tourmaline is widespread in the Li-rich pegmatite this study (Fig. 2b, c, f, h, and i). Already in hand samples different generations of tourmaline could be distinguished by a different color spectrum. Under plane-polarized light in the polarizing microscope they display different colors and partly a strong pleochroism; under crossed polars the respective interference colors are also slightly different (Fig. 2h and 3a-b). According to the different optical characteristics, all tourmalines in the sample can be divided into four generations: Tur-1 exhibits the darkest (brownish) colors in plane polarized light and forms the core of zoned crystal (Fig. 2h and 3b). It is surrounded by Tur-2, which displays a lighter brown color followed by a thin generation of a light brownish Tur-3 formed during relatively later (Fig. 3b). Tur-4 envelopes Tur 3 (Fig. 3b) and is widely distributed in the pegmatite matrix forming

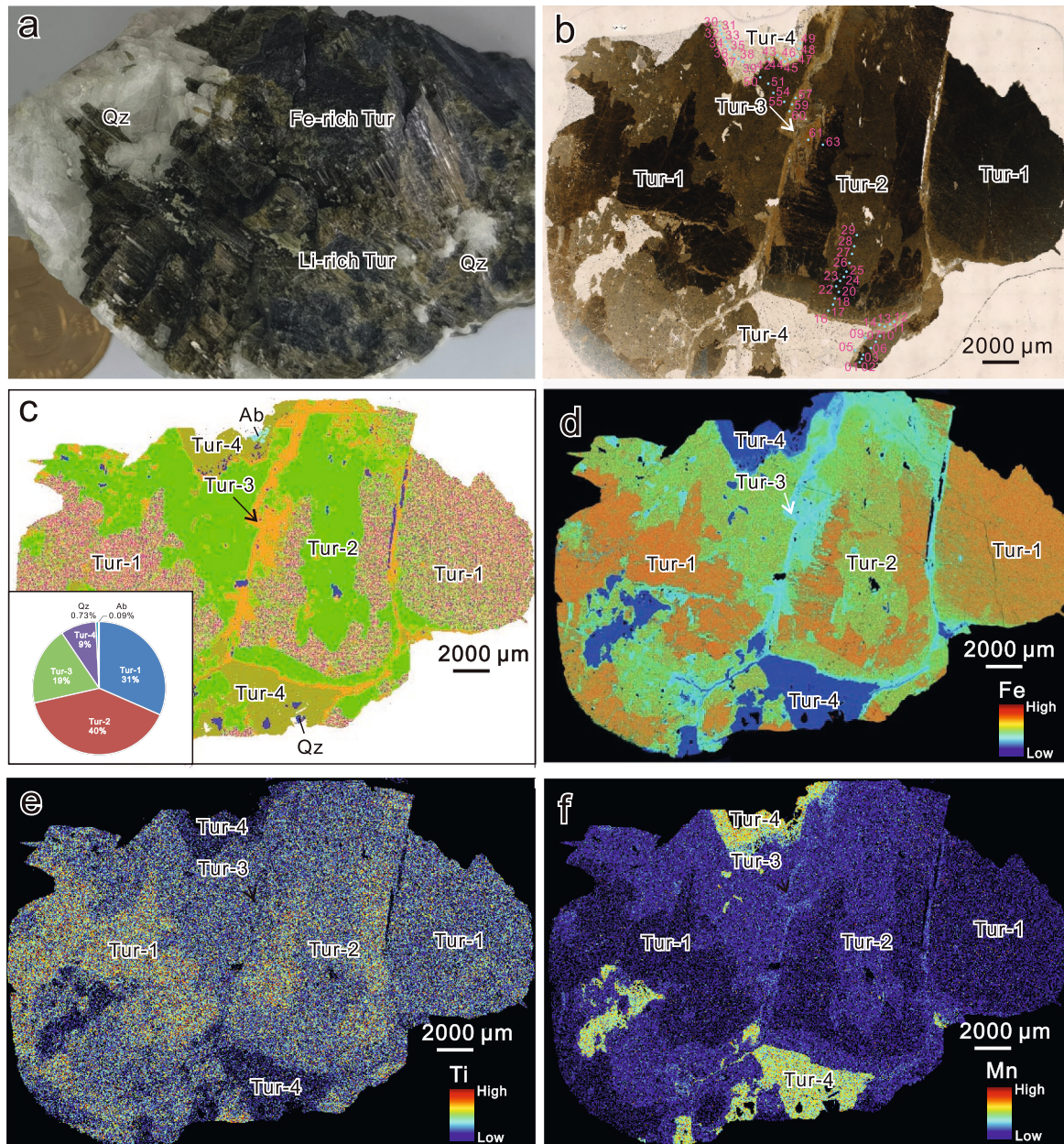


Fig. 3. (a-b) Photograph shows four generations of tourmaline in the Li-rich pegmatite; (c) TIMA image shows the proportion of minerals in the Li-rich pegmatite; Fe (d), Ti (e), and Mn (f) elemental mappings of four generations of tourmaline. Qz-quartz; Tur-tourmaline; Ab-albite.

single grains as well as intergrowth textures with porphyritic K-feldspar and plagioclase (Fig. 2f, h, and i); this type exhibits the lightest color among the tourmaline generations. Tur-4 frequently fills interstices (Fig. 3d), suggesting that the growth of this generation represents the final stage of crystallization or at hydrothermal stage. Boundaries between different tourmaline zones are abrupt, and occasionally earlier tourmaline generations appear to have been partially resorbed prior to the growth of a later generation, producing irregular surfaces or embayments (Fig. 3b).

Detailed TIMA analysis indicates that the tourmaline aggregates consist of Tur-1 (31 vol%), Tur-2 (40 vol%), Tur-3 (19 vol%), Tur-4 (9 vol%), quartz (0.73 vol%), albite (0.09 vol%), and minor amounts of apatite, rutile, and columbite (Fig. 3c). In the mapping diagram (Fig. 3d-f) an episodic decrease in Fe and Ti content becomes apparent, while there is an episodic increase in Mn content from Tur-1 to Tur-4.

The four generations of tourmaline show large variations in Al_2O_3 (32.8–38.0 wt%), FeO (2.20–13.8 wt%), and MnO (0.50–4.52 wt%)

(Table S1). From Tur-1 to Tur-4, the content of FeO decreases, while the contents of Al_2O_3 and MnO increase. Smaller variations are observed for SiO_2 (31.0–36.6 wt%), CaO (0.01–0.39 wt%), Na_2O (2.54–3.73 wt%), TiO_2 (0.09–0.87 wt%), and MgO (0.03–0.34 wt%) (Table S1). According to the Ca-X site vacancy-Na(+K) ternary diagram (Fig. 4a; Henry et al., 2011), the four generations of tourmaline belong to alkali group tourmaline. They fall between the schorl (Fe-rich) and elbaite (Li-rich) end members (Fig. 4b-c). Tur-1 and Tur-2 belong to the $(\text{Na} + \text{K})\text{-R}^{2+}$ species and plot in the field of schorl on the Li-Fe-Mg ternary diagram (Fig. 4b-c; Henry and Guidotti, 1985). Tur-3 and Tur-4 belong to the $(\text{Na} + \text{K})\text{-Li}$ species and plot in the field of elbaite on the Li-Fe-Mg ternary diagram (Fig. 4b, c). On the ternary provenance Al-Fe-Mg diagram (Fig. 4d), all tourmalines plot in the field of Li-bearing granitoids and associated pegmatite and aplites.

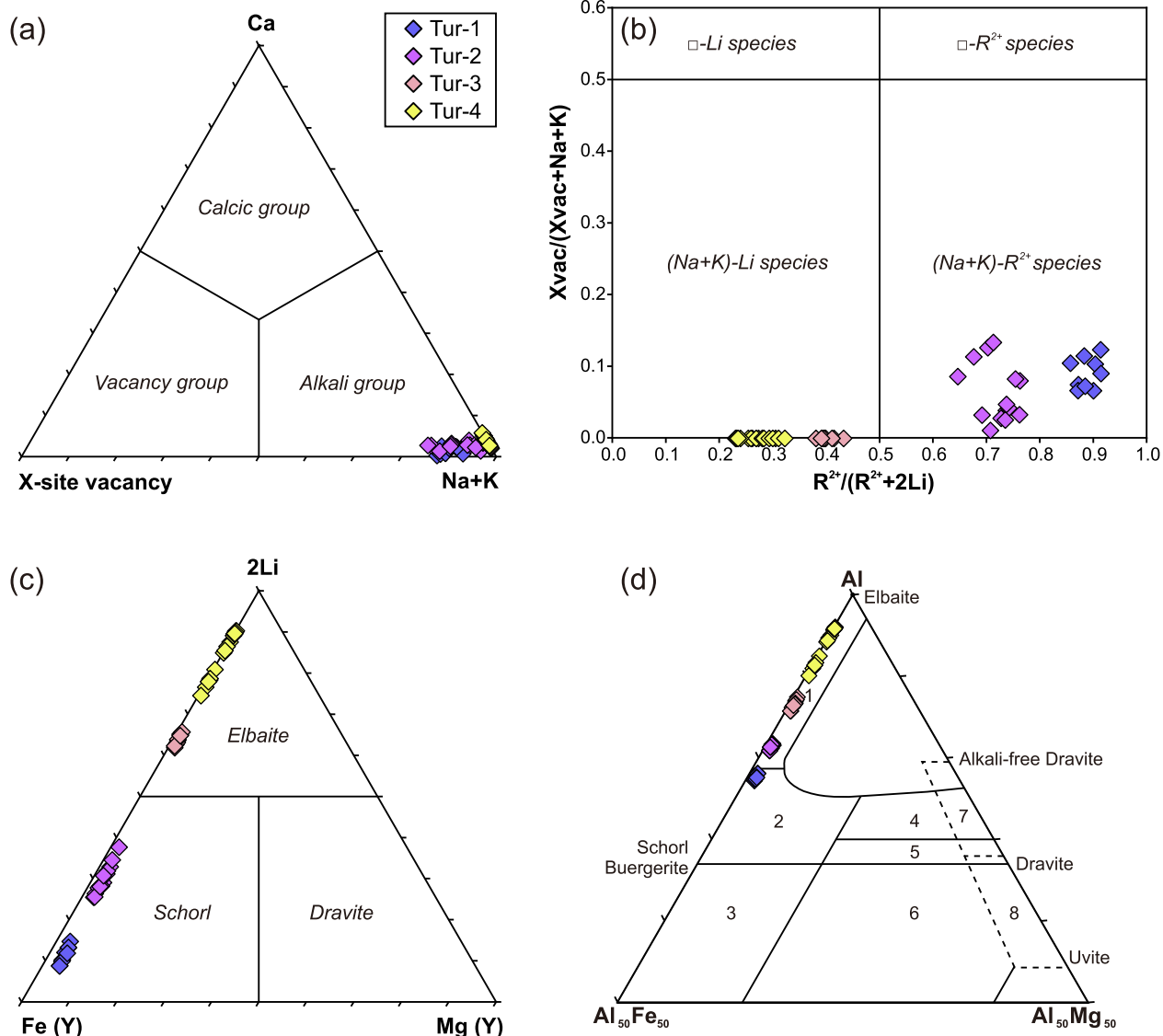


Fig. 4. Chemical compositions of four generations of tourmaline in the Li-rich pegmatite. (a) Classification of the principal groups of tourmaline in $(\text{Na} + \text{K})\text{-Ca-Xvac}$ ternary diagram (Hawthorne and Henry, 1999); (b) Variations in $\text{R}^{2+}/(\text{R}^{2+}+2\text{Li})$ vs $X_{\text{vac}}/(X_{\text{vac}}+\text{Na} + \text{K})$ (Henry et al., 2011); (c) Li-Fe-Mg ternary diagrams (Henry et al., 2011); (d) Al-Fe-Mg diagram (Henry and Guidotti, 1985). Labeled fields are (1) Li-rich granitoid pegmatites and aplites; (2) Li-poor granitoids, pegmatites, and aplites; (3) Fe^{3+} -rich quartz-tourmaline rocks (altered granitoids); (4) metapelites and metapsammites with Al-saturating phase; (5) metapelites and metapsammites lacking Al-saturating phase; (6) Fe^{3+} -rich quartz-tourmaline rocks, calc-silicate rocks, and metapelites; (7) low-Ca metalultramafic rocks and Cr-V-rich metasediments; and (8) metacarbonates and metapyroxenites.

4.2. Trace element compositions

Most of the trace elements are present close to or below their detection limits. However, certain trace elements, such as Li (656–10,055 ppm), Be (5.02–18.8 ppm), K (37.7–83.6 ppm), Ge (1.99–17.1 ppm), Sn (19.2–119 ppm), Nb (0.17–1.20 ppm), Ta (0.35–1.86 ppm), and Pb (0.91–71.6 ppm), can be detected. The Li element exhibits changes spanning several orders of magnitude (Table S1). Variation diagrams of selected trace elements versus FeO are presented in Fig. 5. From Tur-1 to Tur-4, the concentrations of Li, Be, Pb, and Ge generally exhibit gradual increases, while those of Sn and Ti generally decrease (Fig. 5f-g). Regarding Nb and Ta, from Tur-1 to Tur-3 Nb shows a continuous decrease while Ta remains relatively constant, leading to a decreasing Nb/Ta ratio (Fig. 5i). However, from Tur-3 to Tur-4, both Nb and Ta remain relatively constant, resulting in a consistent Nb/Ta ratio (Fig. 5i).

4.3. Boron isotope composition

Boron isotope compositions of the tourmaline generations are provided in Table S2 and depicted in Fig. 7. These display a moderate variation in boron isotopic compositions, with $\delta^{11}\text{B}$ values ranging from −12.0 to −10.8 ‰ for Tur-1, −11.7 to −10.9 ‰ for Tur-2, −11.6 to −10.9 ‰ for Tur-3, and −12.4 to −11.1 ‰ for Tur-4. In general, all 4 generations document a considerable overlap in $\delta^{11}\text{B}$ and only a few

analyses of Tur-4 are lower in $\delta^{11}\text{B}$ compared to the earlier generations Tur-1 to Tur-3 (Fig. 7).

5. Discussion

5.1. Origin and composition of tourmaline and its implication for pegmatite evolution

In this study area, four generations of zoned tourmaline from a single pegmatite vein were investigated using major, and trace element analyses, as well as boron isotope analysis. These tourmalines are subhedral to euhedral and exhibit no signs of alteration. They coexist with plagioclase, quartz, and K-feldspar, displaying sharp contacts (Figs. 2 and 3), which supports their magmatic origin. The magmatic origin of these tourmalines is also supported by a high Na/(Na + Ca) ratio (0.904–0.995), elevated Al contents in the Y sites (0.490–0.99 apfu), and extremely low Mg/(Mg + Fe) ratios (0.01–0.02), which are indicative of syn-magmatic tourmalines (Fig. 4c-d; Table S1; Cheng et al., 2021; Huan et al., 2023; London and Manning, 1995). The $\delta^{11}\text{B}$ values range from −12.4 ‰ to −10.8 ‰ in the four generations of tourmaline (Fig. 7; Table S2), which fall within a narrow range typical of boron isotope compositions found in continental crust, granites, pegmatites, and S-type granites globally (Marschall and Jiang, 2011; Trumbull et al., 2020). This characteristic suggests that the tourmaline originates from a magmatic source associated with a shared peraluminous reservoir.

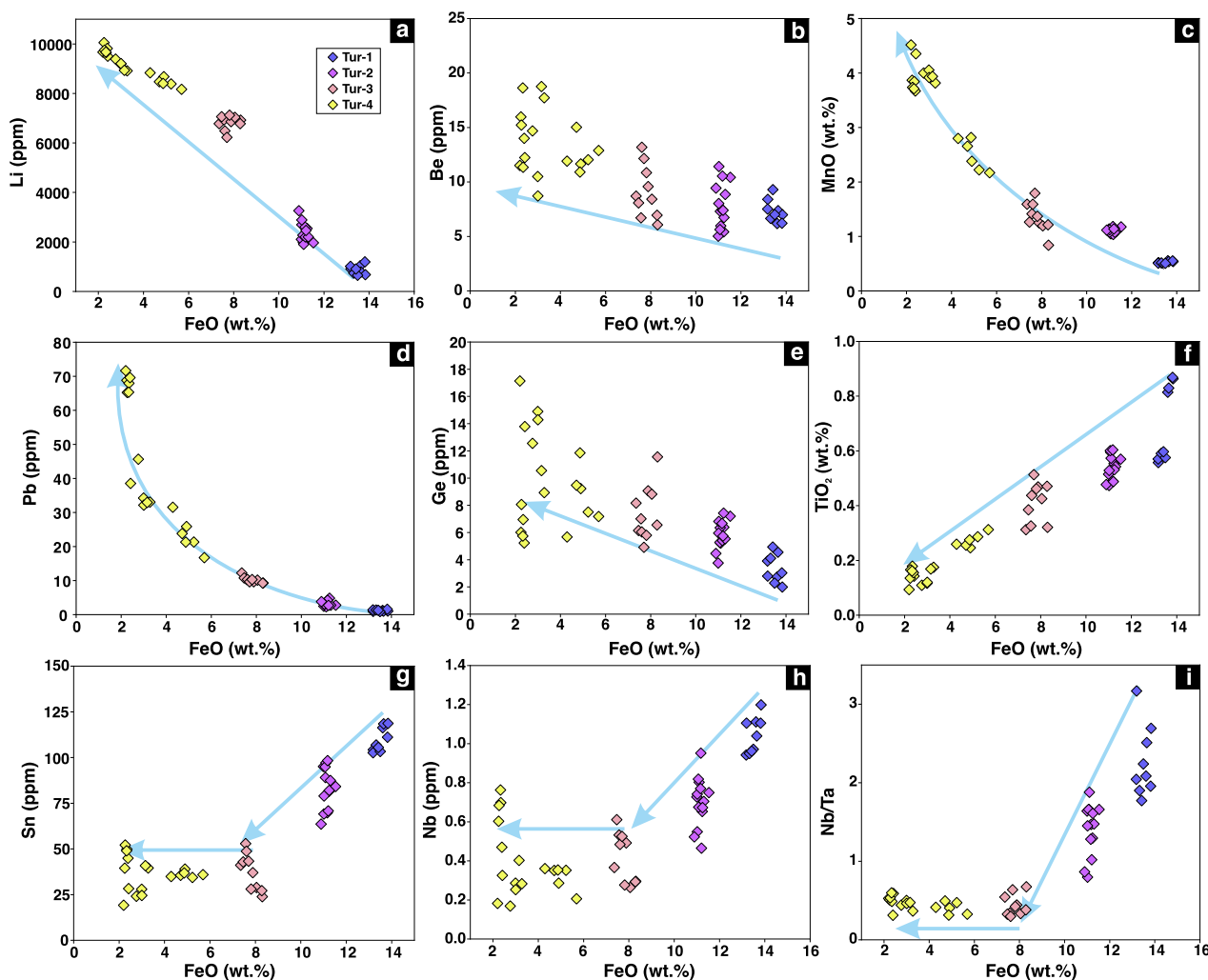


Fig. 5. Compositional variation diagrams for four generations of tourmaline from the Li-rich pegmatite showing the FeO vs. Li, Be, MnO, Pb, Ge, TiO₂, Sn, Nb, and Nb/Ta.

Notably, the FeO content in the tourmalines decreases with pegmatite evolution, as documented in several pegmatite studies (Sun et al., 2024). From Tur-1 to Tur-4, the decreasing FeO content indicates that the crystallization sequence from Tur-1 to Tur-4 occurs progressively later (Fig. 5). Previous research has shown that the major and trace element compositions of magmatic tourmaline reflect the characteristics of the melt from which they crystallized, capturing relevant geological processes (Launay et al., 2018; Li et al., 2022; Sciuba et al., 2021; van Hinsberg et al., 2011). Therefore, the relatively chronological sequence of these four distinguished generations of tourmaline is expected to contribute significantly to deciphering the process of magma evolution.

Early-stage Tur-1 and Tur-2 are relatively Fe-rich schorls, belonging to the $(\text{Na} + \text{K})\text{-R}^{2+}$ species (Fig. 4b) and exhibit high Xvac and low Li and Al contents (Fig. 4c-d). Tur-3 and Tur-4, demonstrate decreasing Fe content and Xvac, alongside increasing Li and Al contents; their compositions belong to the elbaite (Li-rich) and $(\text{Na} + \text{K})\text{-Li}$ species (Fig. 4b). The episodic decrease in Fe and increase in Li and Al from Tur-1 to Tur-4 types, indicate a shift of Li enrichment and Fe-depletion during magma evolution.

During the fractionation of pegmatitic melt, incompatible trace elements such as Li, Be, Nb, Ta, Pb, and Mn become progressively enriched in the residual melt (Chakraborty et al., 2023; van der Does et al., 2024). Consequently, the relative concentrations of these elements in tourmaline can serve as indicators of the magma's evolutionary history and the degree of fractionation (Chakraborty et al., 2023; Jolliff et al., 1986; Roda-Robles et al., 2015). In our analysis, the contents of Li, Be, Mn, Pb, and Ge show a near-linear episodic increase from Tur-1 to Tur-4 (Fig. 5a-e). Conversely, Ti, Sn, and Nb — also incompatible elements (Chakraborty et al., 2023) — exhibit a decreasing trend from Tur-1 to Tur-4 (Fig. 5f-h). This trend suggests that the contemporaneous crystallization of accessory minerals such as rutile, columbite, and cassiterite during magma evolution influences the behavior of these elements in tourmaline (Ballouard et al., 2016; Chevchelov, 2005; Martins et al., 2011). Notably, during the late stages of magma evolution, particularly with the formation of Tur-3 and Tur-4, the concentrations of Sn and Nb, as well as the Nb/Ta ratios, remain stable (Fig. 5g-i). This stability indicates that the concentrations of Sn and Nb in the melt at these stages were insufficient to trigger the crystallization of columbite and cassiterite (Fig. 5a). It further supports the notion that Nb-Ta and Sn mineralization generally occurs in the earlier stages of magma evolution, preceding the mineralization of Li (Shearer et al., 1992). The continuous increase in Be from Tur-1 to Tur-4 can be attributed to its inherent properties and the absence of abundant Be-rich minerals, such as beryl, phenacite, and chrysoberyl (Fig. 5b). Thin section studies reveal that Be mineralization commenced almost concurrently with the formation of elbaites in the late stages of magma evolution (Fig. 2i). From this analysis, we propose a relative chronological sequence for mineralization in the Nassarawa pegmatites, ranging from early to late elements: Nb-Ta-Sn-Be-Li. This pattern aligns with previously established mineralization zones in pegmatites (Martins et al., 2011), suggesting that different mineralization types within unzoned pegmatites have a relative chronological relationship rather than forming simultaneously. Thus, we conclude that extensive fractional crystallization of the magmatic reservoir plays a crucial role in the formation of lithium-rich pegmatites in the Nassarawa region.

5.2. Pulsed magmatic melt releases for the formation of lithium-rich pegmatites

Our study supports the notion that highly differentiated magma is crucial for concentrating rare metals to potentially economic levels, yet the specific processes of magma evolution — such as segregation, ascent, and emplacement — remain unclear. The zoning of tourmaline growth can provide valuable insights into the processes occurring within the magma chamber (Cheng et al., 2021). Continuous fractional crystallization can result in crystals that lack zoning or show gradual variations

in chemical composition (Ginibre et al., 2007; Streck, 2008). In pegmatitic systems, Li exhibits a lower affinity than potassium (K) for common minerals like feldspar and mica. Lithium tends to concentrate in highly evolved melts, while potassium is more readily incorporated into feldspar and mica (Breiter et al., 2019; Philpotts and Schnetzler, 1970). Consequently, a high Li/K ratio and low K concentration reflect a greater degree of magmatic differentiation in lithium-enriched pegmatites (Fig. 6a). Germanium (Ge) behaves similarly to lithium (Höll et al., 2007), not easily incorporating into common pegmatitic minerals. As magma evolves, the concentrations of both lithium and germanium increase (Fig. 6b). Scandium (Sc), being a compatible element relative to lithium, is more easily incorporated into mineral phases (Higuchi and Nagasawa, 1969). Therefore, as magma evolves, lithium concentrations rise while scandium concentrations decrease, resulting in a high Li/Sc ratio and low scandium content in highly evolved melts (Fig. 6c). Element ratios sensitive to magmatic evolution, such as Zr/Hf versus Hf in zircon and K/Rb versus Rb, K/Cs versus Cs in muscovite, are often used to assess the degree and process of magma differentiation (Chakraborty et al., 2023; Wang et al., 2010). If the four generations of tourmaline had undergone a continuous crystallization process, their Li/Sc versus Sc, Li/Ge versus Ge, and Li/K versus K relationships should form continuous, nearly complete curves indicative of rayleigh fractionation. Instead, our data reveals four distinct Rayleigh fractionation curves, suggesting that these generations of tourmaline did not form through a continuous crystallization process (Fig. 6). Two possible explanations for this observation are: (1) Melts from different sources or distinct magmatic settings result in compositional variations in the melt (van der Does et al., 2024), and (2) The evolution of pulsed melts from the same magma reservoir at varying degrees of evolution. Nevertheless, the $\delta^{11}\text{B}$ values ranging from -12.4 ‰ to -10.8 ‰ in the four generations of tourmaline (Fig. 7; Table S2) indicate a narrow range, suggesting that all these tourmalines share a common origin.

Magmatic recharge from a common source can induce significant changes, leading to episodic elemental compositional zoning in minerals (Streck, 2008). Variations in pressure-temperature conditions, along with differing melt compositions, can trigger mineral resorption followed by renewed crystallization (Singer et al., 1995; Streck, 2008). The studied tourmalines display diverse chemical zoning (Fig. 3d-f) and variations in elemental concentrations across different domains (Fig. 6). These variations, sometimes accompanied by resorption-precipitation textures, suggest that diverse melt compositions are primarily influenced by multistage magma injections, facilitating the incremental growth of tourmaline in equilibrium with the respective melt. The narrow $\delta^{11}\text{B}$ values observed across the four tourmaline generations indicate that they formed from a single magmatic reservoir, with no significant melt recharge events from external sources. This implies that the data reflect episodic magma pulses originating from a singular, cooling magma reservoir. Early-stage magma pulses underwent low fractional crystallization, allowing these melts to percolate and interact with crystals within a relatively small magmatic mush. This interaction produced crystals with disequilibrium textures, such as partial resorption, and modified the local bulk composition, leading to local compositional heterogeneities. In contrast, the high degree of fractionation in the underlying cooling magmatic reservoir results in elevated concentrations of certain incompatible trace elements, such as Li and Be, becoming enriched in the later-stage pulses compared to the earlier ones.

Boron exists in two isotopes: ^{11}B and ^{10}B (Trumbull and Slack, 2018). Magmatic fluids are typically more enriched in ^{11}B compared to the associated granitic melts and boron-bearing minerals (e.g., Meyer et al., 2008; Wunder et al., 2005; Maner IV and London, 2018). Consequently, liquid exsolution during pegmatite evolution can lead to a reduction in the $\delta^{11}\text{B}$ isotope values of the residual melt phase (Trumbull et al., 2013). In pegmatite systems, mica and tourmaline are the primary boron-bearing minerals (Trumbull et al., 2013). The crystallization of tourmaline results in a decrease in the $\delta^{11}\text{B}$ value of the residual melt,

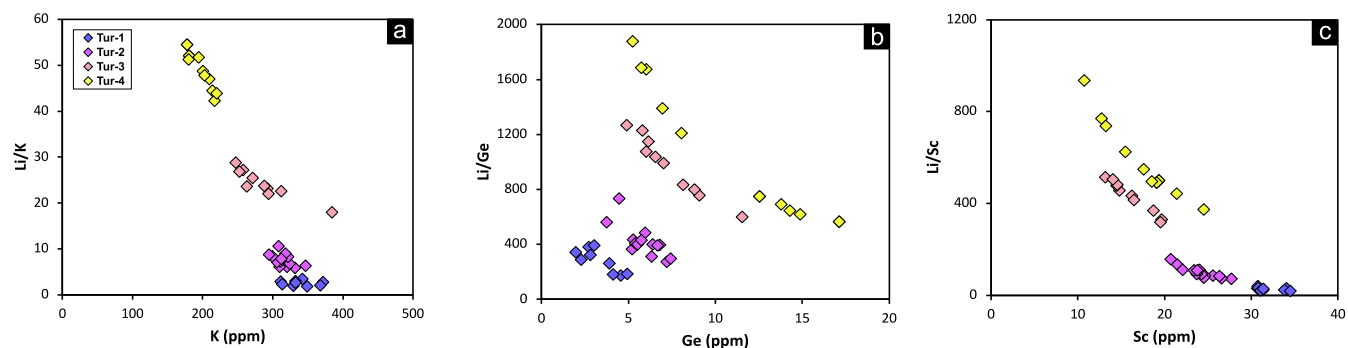


Fig. 6. Compositional variation diagrams for four generations of tourmaline from the Li-rich pegmatite showing the Li/K vs K, Li/Ge vs Ge, and Li/Sc vs Sc.

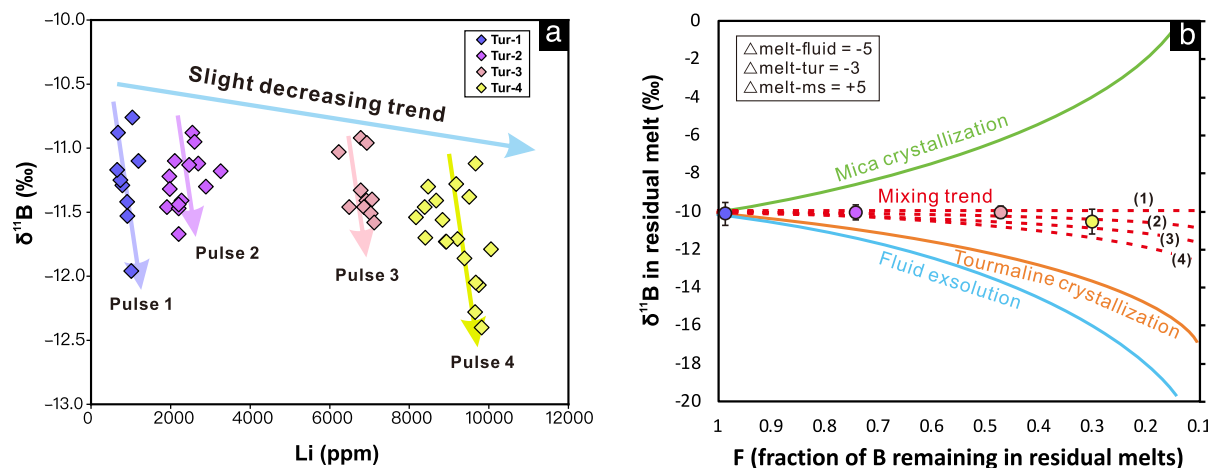


Fig. 7. (a) Plot diagram of $\delta^{11}\text{B}$ values vs. Li for four generations of tourmaline (b). Modeled curves illustrating the change of $\delta^{11}\text{B}$ values for residual melts of pegmatite as the result of tourmaline/muscovite crystallization and a fluid phase exsolution, assuming Rayleigh fractionation. The values of $\Delta^{11}\text{B}$ melt-fluid, $\Delta^{11}\text{B}$ melt-tourmaline, and $\Delta^{11}\text{B}$ melt-muscovite are from Trumbull et al. (2013). The $\delta^{11}\text{B}$ value at $F = 1.0$ for the initial melt of the pegmatite is calculated based on the minimum $\delta^{11}\text{B}$ values determined of the Tur-1 (-10 ‰). (1), (2), (3), and (4) represent that the mass ratio of tourmaline, muscovite, and fluid exsolution is 0.25:0.45:0.3, 0.3:0.4:0.3, 0.4:0.35:0.25, 0.4:0.3:0.3, respectively.

whereas the crystallization of mica leads to an increase in the $\delta^{11}\text{B}$ value (Trumbull et al., 2013). In examining the four generations of tourmaline, Tur-1 to Tur-3 show nearly consistent $\delta^{11}\text{B}$ values, with only Tur-4 exhibiting a slight decrease (Fig. 7a). This trend can be attributed to two potential mechanisms: (1) a phase that removes more ^{11}B from the pegmatite-forming melt occurs only during the crystallization of Tur-4, or (2) a new melt with a relatively unchanged $\delta^{11}\text{B}$ value experiences a slight decrease during the crystallization of Tur-4. If the first scenario is correct, then significant crystallization of B-bearing minerals or fluid exsolution should not have occurred from Tur-1 to Tur-3, which contradicts our sample data (Figs. 2 and 3). Thus, the second explanation may be more plausible. If both exsolution and mineral crystallization influence the $\delta^{11}\text{B}$ fluctuations of the new pulsed melt, a coherent trend across the four tourmaline generations may arise (Fig. 7b). To validate this hypothesis, we employed a Rayleigh fractionation model. The values of $\Delta^{11}\text{B}$ melt-fluid, $\Delta^{11}\text{B}$ melt-tourmaline, and $\Delta^{11}\text{B}$ melt-muscovite (at 500 °C) are sourced from Trumbull et al. (2013). The $\delta^{11}\text{B}$ value for the initial melt of the pegmatite at $F = 1.0$ is calculated based on the minimum $\delta^{11}\text{B}$ values determined for Tur-1 (-10 ‰). The mass ratios of tourmaline, muscovite, and fluid exsolution in the four stages are as follows: (1) 0.25:0.45:0.30, (2) 0.30:0.40:0.30, (3) 0.40:0.35:0.25, and (4) 0.40:0.30:0.30. Our findings indicate that by simultaneously controlling the $\delta^{11}\text{B}$ values of the parent melt through the crystallization of B-bearing minerals and fluid exsolution, the $\delta^{11}\text{B}$

values in the early stages of melt evolution can remain relatively stable, with only slight decreases observed in the later stages (Fig. 7b). With the $\delta^{11}\text{B}$ of the parental magma remaining nearly constant (Fig. 7b), each generation of tourmaline exhibits a negative correlation between B isotopes and Li content (Fig. 7a). This further suggests the formation of unzoned pegmatite-type lithium deposits by multiple magmatic pulses within a progressively cooling parental magma chamber.

We propose a model involving multiple melt-release events from a single cooling magmatic reservoir to explain the formation of lithium-rich pegmatites in the Nassarawa-Keffi area (Fig. 8). This model aligns with the cross-cutting pegmatite veins observed in various deposits, such as those in the Osi Area of Northern Nigeria and Jiajika in Western China (Huang et al., 2020; King, 1948; London, 2018). Our findings indicate that lithium enrichment likely resulted from successive magmatic melt pulses, with each pulse exhibiting increased lithium concentrations linked to fractional crystallization. This interpretation remains preliminary, necessitating further mineral analyses for validation. The traditional view of a singular crystallization event fails to explain the distinct zoning in the tourmaline generations and the abrupt elemental variations. In contrast, our model addresses these complexities, offering insights into the unzoned pegmatites of Nassarawa area (Fig. 8). Similar unzoned pegmatites documented in regions like North Carolina, South Carolina, and Western Australia show a dispersed distribution of rare metal mineralizations rather than confined zones (Liu et al., 2024;

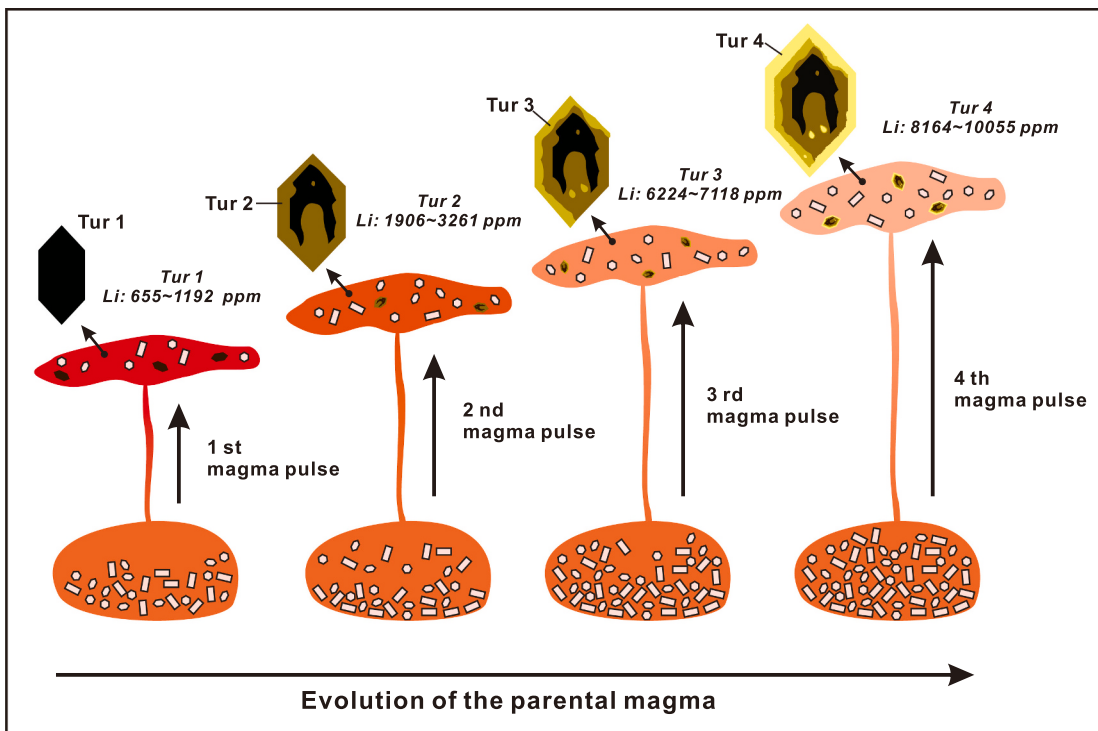


Fig. 8. Schematic diagrams of multiple magma pulses, tourmaline formation, and for the unzoned pegmatite.

Swanson, 2012; Sweetapple et al., 2019). Furthermore, considerable variations in crystallization ages among minerals suggest distinct stages during multiple melt pulses (Ma et al., 2024; Zhu et al., 2023). Thus, our model provides an alternative model in which multiple melt-release events from a single cooling magmatic reservoir contribute to the formation of lithium-rich pegmatites.

6. Conclusion

In-situ analyses of major and trace elements, along with boron isotopes, on at least four generations of tourmaline of a lithium mineralization from the Nassarawa-Keffi pegmatite belt in Nigeria, have provided valuable insights into the complex processes of crystallization and lithium enrichment. The multistage growth zoning observed in tourmaline, documented by specific elements and boron isotopic signatures, signifies a series of intermittent melt flux events rather than a singular continuous crystallization event. The periodic fluctuations in the concentrations of Fe, Li, Be, Ge, Mn, Pb, Nb, and TiO₂, accompanied by changes in δ¹¹B values, suggest the occurrence of at least four distinct pulses of magmatic activity. The later pulses lead to tourmaline domains of higher lithium concentrations, indicating that successive melt injections, coupled with extensive fractional crystallization in a deep magmatic reservoir, play a pivotal role in the lithium enrichment of the rocks. This study advances our understanding of the intricate processes involved in the development of multiple magma pulses within the framework of lithium mineralization in a pegmatitic system, that originates from a single magma reservoir. This model explains the formation of unzoned pegmatites in the Nassarawa area. The comprehension of multistage growth processes of minerals can effectively signify the extent of magmatic differentiation, point to the possible involvement of different magma sources, and facilitate the exploitation of lithium resources in similar geological contexts. However, we must acknowledge the necessity for conducting similar studies involving trace element and isotope geochemical analyses of different mineral species and of tourmaline crystals from different regions of the same pegmatite body, to gain a comprehensive understanding of potential different magma

pulses or pegmatitic-pneumatolytic processes throughout the entire magmatic history to occur.

Supplementary data to this article can be found online at <https://doi.org/10.1016/j.lithos.2024.107936>.

CRediT authorship contribution statement

Junteng Lv: Writing – original draft, Software, Methodology, Conceptualization. **Xin Chen:** Writing – review & editing, Writing – original draft, Software, Methodology, Investigation, Funding acquisition, Conceptualization. **Junsheng Jiang:** Writing – review & editing, Investigation. **Hans-Peter Schertl:** Writing – review & editing, Visualization. **Liang Cao:** Writing – review & editing, Investigation. **Xiaojia Jiang:** Writing – original draft, Methodology, Data curation.

Acknowledgments

We would like to sincerely thank the Editor-in-Chief and Associate Editor of Lithos for their efficient handling of the manuscript and their valuable constructive comments. Our gratitude also extends to the two anonymous reviewers for their helpful suggestions. Funding for this study was provided by the Postdoctoral Science Foundation of China (BX20220277, 2022 M722938), the China Geological Survey Project (DD20230126), and the open fund of the Research Center for Petrogenesis and Mineralization of Granitoid Rocks, China Geological Survey (PMGR202103).

References

- Adetunji, A., Ocan, O.O., 2010. Characterization and mineralization potentials of granitic pegmatites of Komu area, Southwestern Nigeria. *Resour. Geol.* 60 (1), 87–97.
- Ajibade, A., Woakes, M., Rahaman, M., 1987. Proterozoic crustal development in the Pan-African Regime of Nigeria. *Proterozoic Lithospher. Evolut.* 17, 259–271.
- Akintola, A., Ikhane, P., Okunlola, O., Akintola, G., Oyebolu, O., 2012. Compositional features of precambrian pegmatites of Ago-Iwoye area South Western, Nigeria. *J. Ecol. Nat. Environ.* 4 (3), 71–87.
- Ananaba, S., Ajakaiye, D., 1987. Evidence of tectonic control of mineralization in Nigeria from lineament density analysis A Landsat-study. *Int. J. Remote Sens.* 8 (10), 1445–1453.

- Annen, C., 2009. From plutons to magma chambers: Thermal constraints on the accumulation of eruptive silicic magma in the upper crust. *Earth Planet. Sci. Lett.* 284 (3-4), 409–416.
- Arthaud, M.H., Caby, R., Fuck, R.A., Dantas, E.L., Parente, C.V., 2008. Geology of the northern Borborema Province, NE Brazil and its correlation with Nigeria, NW Africa. *Geol. Soc. Lond. Spec. Publ.* 294 (1), 49–67.
- Balouard, C., Poujol, M., Boulvais, P., Branquet, Y., Tartèse, R., Vigneresse, J.-L., 2016. Nb-Ta fractionation in peraluminous granites: A marker of the magmatic-hydrothermal transition. *Geology* 44 (3), 231–234.
- Bradley, D., McCauley, A., 2013. A preliminary deposit model for lithium-cesium-tantalum (LCT) pegmatites. US Geol. Survey. <https://doi.org/10.3133/of20131008>.
- Breiter, K., Hložková, M., Korbelová, Z., Galiová, M.V., 2019. Diversity of lithium mica compositions in mineralized granite-greisen system: Cínovec Li-Sn-W deposit, Erzgebirge. *Ore Geol. Rev.* 106, 12–27.
- Bruguier, O., Dada, S., Lancelot, J., 1994. Early Archaean component (> 3.5 Ga) within a 3.05 Ga orthogneiss from northern Nigeria: U-Pb zircon evidence. *Earth Planet. Sci. Lett.* 125 (1–4), 89–103.
- Cameron, E.N., Jahns, R.H., McNair, A.H., Page, L.R., 1949. Internal structure of granitic pegmatites. *Econom. Geol. Monograph Series* 2, 115.
- Cao, L., Chen, X., Jiang, J., Garba, A.A., Li, H., Chao, N., Hu, P., Lv, X., 2024. Geochronology of cassiterite in the Nassarawa-Keffi rare metal pegmatite belt, Nigeria: Tectonic linkages to the Gondwana-forming orogeny. *Ore Geol. Rev.* 175, 106339.
- Cashman, K.V., Sparks, R.S.J., Blundy, J.D., 2017. Vertically extensive and unstable magmatic systems: a unified view of igneous processes. *Science* 355 (6331), 3055.
- Cerný, P., 1991. Rare-element Granitic Pegmatites. Part I: Anatomy and Internal Evolution of Pegmatitic Deposits. *Geosci. Can.* 18 (2), 49–67.
- Cerný, P., Ercit, T.S., 2005. The classification of granitic pegmatites revisited. *Can. Mineral.* 43 (6), 2005–2026.
- Chakraborty, T., Büttner, S.H., Costin, G., Kankuzi, C.F., 2023. The petrogenesis of highly fractionated gem-bearing pegmatites of Malawi: evidence from mica and tourmaline chemistry and finite step trace element modelling. *Mineral. Deposita* 59 (4), 837–857.
- Chen, J.-Z., Zhang, H., Tang, Y., Lv, Z.-H., An, Y., Wang, M.-T., Liu, K., Xu, Y.-S., 2022. Lithium mineralization during evolution of a magmatic-hydrothermal system: Mineralogical evidence from Li-mineralized pegmatites in Altai, NW China. *Ore Geo. Rev.* 149, 105058.
- Cheng, L., Zhang, C., Liu, X., Yang, X., Zhou, Y., Horn, I., Weyer, S., Holtz, F., 2021. Significant boron isotopic fractionation in the magmatic evolution of Himalayan leucogranite recorded in multiple generations of tourmaline. *Chem. Geol.* 571, 120194.
- Chevychelov, V., 2005. Effect of Melt Composition and Temperature on the Partitioning of Ta, Nb, Mn, and F between Granitic (Alkaline) Melt and Fluorine-Bearing Aqueous Fluid: Fractionation of Ta and Nb and Conditions of Ore Formation in Rare-Metal Granites V. Yu. Chevychelov, G. P. Zaraisky, S. E. Borisovskii, and D. A. Borkov. *Petrology* 13, 305–321.
- Coleman, D.S., Mills, R.D., Zimmerer, M.J., 2016. The pace of plutonism. *Elements* 12 (2), 97–102.
- Dada, S., 1998. Crust-forming ages and Proterozoic crustal evolution in Nigeria: a reappraisal of current interpretations. *Precambrian Res.* 87 (1–2), 65–74.
- Daly, R.A., 1911. The nature of volcanic action. *Proceed. American Acad. Arts Sci.* 47, 47–122.
- Fan, Z.W., Xiong, Y.Q., Shao, Y.J., Wen, C.H., 2022. Textural and chemical characteristics of beryl from the Baishawo Be-Li-Nb-Ta pegmatite deposit, Jiangnan Orogen: Implication for rare metal pegmatite genesis. *Ore Geol. Rev.* 149, 105094.
- Ferré, E., Délérés, J., Bouchez, J.-L., Lar, A., Peucat, J.-J., 1996. The Pan-African reactivation of Eburnean and Archaean provinces in Nigeria: structural and isotopic data. *J. Geol. Soc.* 153 (5), 719–728.
- Fitches, W., Ajibade, A., Egbunifie, I., Holt, R., Wright, J., 1985. Late Proterozoic schist belts and plutonism in NW Nigeria. *J. Geol. Soc.* 142 (2), 319–337.
- Ginibre, C., Wörner, G., Kronz, A., 2007. Crystal zoning as an archive for magma evolution. *Elements* 3 (4), 261–266.
- Goodenough, K., Lustig, P., Roberts, N., Key, R., Garba, A., 2014. Post-collisional Pan-African granitoids and rare metal pegmatites in western Nigeria: Age, petrogenesis, and the ‘pegmatite conundrum’. *Lithos* 200, 22–34.
- Hawthorne, F.C., Henry, D.J., 1999. Classification of the minerals of the tourmaline group. *Eur. J. Mineral.* 11, 201–215.
- Henry, D.J., Guidotti, C.V., 1985. Tourmaline as a petrogenetic indicator mineral - An example from the staurolite-grade metapelites of NW Maine. *Am. Mineral.* 70 (1), 1–15.
- Henry, D.J., Novak, M., Hawthorne, F.C., Ertl, A., Dutrow, B.L., Uher, P., Pezzotta, F., 2011. Nomenclature of the tourmaline-super-group minerals. *Am. Mineral.* 96 (5–6), 895–913.
- Higuchi, H., Nagasawa, H., 1969. Partition of trace elements between rock-forming minerals and the host volcanic rocks. *Earth Planet. Sci. Lett.* 7 (3), 281–287.
- Höll, R., Kling, M., Schroll, E., 2007. Metallogenesis of germanium—A review. *Ore Geol. Rev.* 30 (3–4), 145–180.
- Hou, K., Li, Y., Xiao, Y., Liu, F., Tian, Y., 2010. In situ boron isotope measurements of natural geological materials by LA-MC-ICP-MS. *Chin. Sci. Bull.* 55 (29), 3305–3311.
- Huan, C., Wei, H.-Z., Zhu, W.-B., Palmer, M.R., Lin, H.-F., Zheng, B.-H., Cai, Y., Zuo, D.-S., Wang, J.-L., Xu, Z.-Q., 2023. Boron isotopes in tourmaline from drill core of the Jiajika granitic pegmatite type lithium deposit: Insights for granitic magma evolution and lithium enrichment. *Ore Geol. Rev.* 163.
- Huang, T., Fu, X., Ge, L., Zou, F., Hao, X., Yang, R., Fan, J., 2020. The genesis of giant lithium pegmatite veins in Jiajika, Sichuan, China: Insights from geophysical, geochemical as well as structural geology approach. *Ore Geol. Rev.* 124, 103557.
- Ishikawa, T., Tera, F., 1997. Source, composition, and distribution of the fluid in the Kurile mantle wedge: constraints from across-arc variations of B/Nb and B isotopes. *Earth Planet. Sci. Lett.* 152 (1–4), 123–138.
- Ishikawa, T., Tera, F., Nakazawa, T., 2001. Boron isotope and trace element systematics of the three volcanic zones in the Kamchatka arc. *Geochim. Cosmochim. Acta* 65 (24), 4523–4537.
- Jahns, R.H., Burnham, C.W., 1969. Experimental studies of pegmatite genesis; I, A model for the derivation and crystallization of granitic pegmatites. *Econ. Geol.* 64 (8), 843–864.
- Jolliff, B.L., Papike, J.J., Shearer, C.K., 1986. Tourmaline as a recorder of pegmatite evolution; Bob Ingerson pegmatite, Black Hills, South Dakota. *American Mineral.* 71 (3–4), 472–500.
- Kesler, S.E., Gruber, P.W., Medina, P.A., Keoleian, G.A., Everson, M.P., Wallington, T.J., 2012. Global lithium resources: Relative importance of pegmatite, brine and other deposits. *Ore Geol. Rev.* 48, 55–69.
- King, B.C., 1948. The form and structural features of aplite and pegmatite dikes and veins in the Osi area of the Northern Provinces of Nigeria and the criteria that indicate a nondirectional mode of emplacement. *J. Geol.* 56 (5), 459–475.
- Knoll, T., Huet, B., Schuster, R., Mali, H., Ntaflos, T., Hauzenberger, C., 2023. Lithium pegmatite of anatctic origin—A case study from the Austroalpine Unit Pegmatite Province (Eastern European Alps): Geological data and geochemical modeling. *Ore Geol. Rev.* 154, 105298.
- Koopmans, L., Martins, T., Linnen, R., Gardiner, N.J., Breasley, C.M., Palin, R.M., Groat, L.A., Silva, D., Robb, L.J., 2023. The formation of lithium-rich pegmatites through multi-stage melting. *Geology* 52 (1), 7–11.
- Launay, G., Sizaret, S., Guillou-Frottier, L., Gloaguen, E., Pinto, F., 2018. Deciphering fluid flow at the magmatic-hydrothermal transition: A case study from the world-class Pasanqueira W-Sn-(Cu) ore deposit (Portugal). *Earth Planet. Sci. Lett.* 499, 1–12.
- Li, W., Qiao, X., Zhang, F., Zhang, L., 2022. Tourmaline as a potential mineral for exploring porphyry deposits: A case study of the Bilihe gold deposit in Inner Mongolia, China. *Mineral. Deposita* 57, 61–82.
- Liu, Y., Hu, Z., Gao, S., Günther, D., Xu, J., Gao, C., Chen, H., 2008. In situ analysis of major and trace elements of anhydrous minerals by LA-ICP-MS without applying an internal standard. *Chem. Geol.* 257 (1–2), 34–43.
- Liu, X.-C., Kohn, M.J., Wang, J.-M., He, S.-X., Wang, R.-C., Wu, F.-Y., 2024. Formation of lithium-rich pegmatites via rapid crystallization and shearing—case study from the South Tibetan Detachment, Himalaya. *Earth Planet. Sci. Lett.* 629, 118598.
- London, D., 2018. Ore-forming processes within granitic pegmatites. *Ore Geol. Rev.* 101, 349–383.
- London, D., Manning, D.A., 1995. Chemical variation and significance of tourmaline from southwest England. *Econ. Geol.* 90 (3), 495–519.
- Ma, Y.C., Xu, X.W., Hong, T., Jin, W.K., Li, H., Yang, Z.Q., Liu, S.K., Kang, K., Wang, X.H., Niu, L., 2024. Multiphase evolution of a Li-pegmatite field from the Tashisayi area, Altyn Tagh, NW China: insights from a petrological, geochemical, and geochronological study. *Mineral. Deposita* 59 (5), 863–884.
- Maner IV, J.L., London, D., 2018. Fractionation of the isotopes of boron between granitic melt and aqueous solution at 700° C and 800° C (200 MPa). *Chem. Geol.* 489, 16–27.
- Marschall, H.R., Jiang, S.Y., 2011. Tourmaline Isotopes: No Element Left Behind. *Elements* 7 (5), 313–319.
- Martins, T., Lima, A., Simmons, W.B., Falster, A.U., and Noronha, F., 2011. Geochemical fractionation of Nb-Ta oxides in Li-bearing pegmatites from the Barroso-Alvão pegmatite field, Northern Portugal. *Can. Mineral.*, 49(3), 777–791.
- Menand, T., 2011. Physical controls and depth of emplacement of igneous bodies: A review. *Tectonophysics* 500 (1–4), 11–19.
- Meyer, C., Wunder, B., Meixner, A., Romer, R.L., Heinrich, W., 2008. Boron-isotope fractionation between tourmaline and fluid: an experimental re-investigation. *Contrib. Mineral. Petro.* 156, 259–267.
- Müller, A., Romer, R.L., Pedersen, R.B., 2017. The Sveconorwegian pegmatite province—thousands of pegmatites without parental granites. *Can. Mineral.* 55 (2), 283–315.
- Okunola, O., Somorin, E., 2006. Compositional features of Precambrian pegmatites of Itakpe area, central Nigeria. *Glob. J. Geol. Sci.* 4 (2), 221–230.
- Philpotts, J.A., Schnetzler, C.C., 1970. Phenocryst-matrix partition coefficients for K, Rb, Sr and Ba, with applications to anorthosites and basalt genesis. *Geochim. Cosmochim. Acta* 34 (3), 307–322.
- Roda-Robles, E., Simmons, W., Pesquera, A., Gil-Crespo, P.P., Nizamoff, J., Torres-Ruiz, J., 2015. Tourmaline as a petrogenetic monitor of the origin and evolution of the Berry-Havey pegmatite (Maine, USA). *Am. Mineral.* 100 (1), 95–109.
- Sciuba, M., Beaudoin, G., Makvandi, S., 2021. Chemical composition of tourmaline in orogenic gold deposits. *Mineral. Deposita* 56, 537–560.
- Shearer, C.K., Papike, J.J., Jolliff, B.L., 1992. Petrogenetic links among granites and pegmatites in the Harney Peak rare-element granite-pegmatite system, Black Hills, South Dakota. *Canadian Mineralogist* 30, 785–785.
- Singer, B.S., Dungan, M.A., and Layne, G.D., 1995. Textures and Sr, Ba, Mg, Fe, K, and Ti compositional profiles in volcanic plagioclase: clues to the dynamics of calc-alkaline magma chambers. *Am. Mineral.*, 80(7–8), 776–798.
- Streck, M.J., 2008. Mineral textures and zoning as evidence for open system processes. *Rev. Mineral. Geochem.* 69 (1), 595–622.
- Sun, W., Zhao, Z., Mo, X., Dong, G., Li, X., Yuan, W., Wang, T., Wang, B., Pan, T., Han, J., Zheng, F., Tang, Y., 2024. Tourmaline as an indicator for pegmatite evolution and exploration: A case study from the Chakabeishan deposit, northeastern Tibetan Plateau. *Ore Geol. Rev.* 165, 105892.
- Swanson, S.E., 2012. Mineralogy of spodumene pegmatites and related rocks in the tin-spodumene belt of North Carolina and South Carolina, USA. *Can. Mineral.* 50 (6), 1589–1608.

- Sweetapple, M.T., Grigson, M.W., Tornatora, P., Urgine, S., 2019. The Archean Mt. Cattlin spodumene pegmatite group and 3D geochemical mapping of large “unzoned” pegmatites of economic significance. *Can. Mineral.* 57 (5), 803–805.
- Trumbull, R.B., Slack, J.F., 2018. Boron isotopes in the continental crust: granites, pegmatites, felsic volcanic rocks, and related ore deposits. *Boron Isotop.: Fifth Element* 249–272.
- Trumbull, R.B., Beurlen, H., Wiedenbeck, M., Soares, D.R., 2013. The diversity of B-isotope variations in tourmaline from rare-element pegmatites in the Borborema Province of Brazil. *Chem. Geol.* 352, 47–62.
- Trumbull, R.B., Codeço, M.S., Jiang, S.-Y., Palmer, M.R., Slack, J.F., 2020. Boron isotope variations in tourmaline from hydrothermal ore deposits: A review of controlling factors and insights for mineralizing systems. *Ore Geol. Rev.* 125.
- van der Does, L.M., Hulsbosch, N., Kaskes, P., Elsen, J., Claeys, P., Muchez, P., Sirbescu, M.-L.C., 2024. Tourmaline growth in the border and wall zones of the Emmons pegmatite (Maine, USA): Evidence for disequilibrium crystallization and boundary layer formation. *Am. Mineral.* 109 (4), 785–798.
- van Hinsberg, V.J., Henry, D.J., Marschall, H.R., 2011. Tourmaline: an ideal indicator of its host environment. *Can. Mineral.* 49 (1), 1–16.
- Vigneresse, J.L., 2008. Granitic batholiths: from pervasive and continuous melting in the lower crust to discontinuous and spaced plutonism in the upper crust. *Earth Environ. Sci. Trans. Royal Soc. Edinburgh* 97 (4), 311–324.
- Vigneresse, J.-L., 2015. Textures and melt-crystal-gas interactions in granites. *Geosci. Front.* 6 (5), 635–663.
- Vincent, V.I., Wang, L.-X., Zhu, Y.-X., Kamaunji, V.D., Ahmed, H.A., Ntekim, E.E., Cao, L., 2022. Onset of the anorogenic alkaline magmatism in the Nigerian Younger Granite province: Constraints from the Daura and Dutse complexes. *Lithos* 410, 106561.
- Wang, X., Griffin, W.L., Chen, J., 2010. Hf contents and Zr/Hf ratios in granitic zircons. *Geochim. J.* 44 (1), 65–72.
- Wu, F.-Y., Liu, X.-C., Liu, Z.-C., Wang, R.-C., Xie, L., Wang, J.-M., Ji, W.-Q., Yang, L., Liu, C., Khanal, G.P., 2020. Highly fractionated Himalayan leucogranites and associated rare-metal mineralization. *Lithos* 352, 105319.
- Wunder, B., Meixner, A., Romer, R.L., Wirth, R., Heinrich, W., 2005. The geochemical cycle of boron: constraints from boron isotope partitioning experiments between mica and fluid. *Lithos* 84 (3–4), 206–216.
- Xiong, Y.Q., Fan, Z.W., Yu, H.Y., Di, H., Cao, Y.H., Wen, C.H., Jiang, S.Y., 2024. Genetic linkage between parent granite and zoned rare metal pegmatite in the Renli-Chuanziyuan granite-pegmatite system. *Geological Society of America Bulletin*, South China. <https://doi.org/10.1130/B37688.1>.
- Yang, Y., Wang, D., Liu, S., Liu, L., Wang, C., Guo, W., 2020. The co-occurrence mechanism of two types of spodumene ore bodies and their prospecting significance in Jiajikan, Sichuan Province. *Acta Geol. Sin.* 94 (1), 287–302.
- Zhu, J., Zhu, W., Xu, Z., Zhang, R., Che, X., Zheng, B., 2023. The geochronology of pegmatites in the Jiajika lithium deposit, western Sichuan, China: Implications for multi-stage magmatic-hydrothermal events in the Songpan-Ganze rare metal metallogenic belt. *Ore Geol. Rev.* 105582.